ANZIAM J. **67, e18** (2025), 1–22
doi:10.1017/S1446181125000082

GENERIC PLANAR PHASE RESETTING NEAR A PHASELESS POINT

K. H. LEE[1], N. G. R. BRODERICK[2], B. KRAUSKOPF[1] and H. M. OSINGA[1]✉

(Received 21 October, 2024; accepted 29 January, 2025)

Abstract

We study the planar FitzHugh–Nagumo system with an attracting periodic orbit that surrounds a repelling focus equilibrium. When the associated oscillation of the system is perturbed, in a given direction and with a given amplitude, there will generally be a change in phase of the perturbed oscillation with respect to the unperturbed one. This is recorded by the phase transition curve (PTC), which relates the old phase (along the periodic orbit) to the new phase (after perturbation). We take a geometric point of view and consider the phase-resetting surface comprising all PTCs as a function of the perturbation amplitude. This surface has a singularity when the perturbation maps a point on the periodic orbit exactly onto the repelling focus, which is the only point that does not return to stable oscillation. We also consider the PTC as a function of the direction of the perturbation and present how the corresponding phase-resetting surface changes with increasing perturbation amplitude. In this way, we provide a complete geometric interpretation of how the PTC changes for any perturbation direction. Unlike other examples discussed in the literature so far, the FitzHugh–Nagumo system is a generic example and, hence, representative for planar vector fields.

2020 *Mathematics subject classification*: primary 34C15; secondary 37C27, 65L10, 92B25.

Keywords and phrases: Phase transition curve, isochrons, phase-resetting surface, phase singularity.

1. Introduction

Phase resetting is a technique that is often applied in neuroscience to study the behaviour and properties of neuronal firing patterns [4, 18]. In essence, given a stable

[1]Department of Mathematics and Dodd–Walls Centre for Photonic and Quantum Technologies, University of Auckland, Private Bag 92019, Auckland 1142, New Zealand;
e-mail: kyoung.hyun.lee@auckland.ac.nz, b.krauskopf@auckland.ac.nz, h.m.osinga@auckland.ac.nz
[2]Department of Physics and Dodd–Walls Centre for Photonic and Quantum Technologies, University of Auckland, Private Bag 92019, Auckland 1142, New Zealand; e-mail: n.broderick@auckland.ac.nz

oscillation, denoted Γ, a phase reset is the act of applying a perturbation of a particular strength, in a particular direction, and recording the resulting phase shift upon return to Γ with respect to the phase at which the perturbation was applied. Phase resetting is strongly related to the notion of isochrons, which each comprise all points that converge to Γ with a given phase: the phase reset maps a point on Γ to a perturbed point that lies on a particular isochron and, hence, returns to Γ with the phase associated with this isochron. Winfree devoted most of his career to the study of isochrons and the properties of so-called phase-transition and phase-response curves, which relate the "old" phase ϑ_o along Γ to the "new" phase ϑ_n and phase shift $\vartheta_n - \vartheta_o$, respectively, that result from a given fixed perturbation [22]. Winfree defined the old and new phases as fractions of the total time needed to complete one oscillation; hence, $\vartheta_o, \vartheta_n \in [0, 1)$ are defined on the circle $\mathbb{S}^1 := \mathbb{R}/\mathbb{Z}$.

Winfree's classical paper on isochrons [20] defines a *latent* phase for each point in the basin of attraction of Γ for a given system of first-order differential equations (a vector field). Winfree made a series of conjectures regarding the properties of isochrons that were later confirmed by Guckenheimer [7] who realized that isochrons are, in fact, stable manifolds of fixed points given by the fixed-time return map associated with the period T_Γ of Γ. Normally hyperbolic invariant manifold theory [10], which at the time was still being developed, implies that the family of isochrons, parametrized by the phase $\vartheta_o \in [0, 1)$, foliates the basin of attraction of Γ; this means that any point in the basin lies on exactly one isochron (of a specific phase) in the family. Since isochrons are global invariant manifolds, they are not known analytically (except in very special cases) and need to be computed with advanced numerical tools [12, 16].

In this paper, we study instantaneous phase resets for the FitzHugh–Nagumo system [5, 15], which is a planar, polynomial system that will be introduced in the next section; see already system (2.1). More precisely, the perturbation applied at the moment of resetting is a Dirac delta function that instantaneously and discontinuously shifts the state to a different point in the plane, as given by the size and direction of the reset. The parameters for the FitzHugh–Nagumo system are chosen such that it has an attracting periodic orbit Γ and our interest lies in the possible behaviour of its phase transition curves (PTCs) that relate the new phase ϑ_n to the old phase ϑ_o before the reset. Note that, certainly for planar systems, not all points in the phase space converge to Γ and phase resets are meant to involve only resets to points in the basin of attraction of Γ; discontinuities arise when resets occur to points in the so-called phaseless set, which consists of all points outside of the basin of attraction. For the FitzHugh–Nagumo system, we encounter a phaseless set that is quite typical for planar vector fields [12, 14, 16]: it comprises a single point, denoted $\boldsymbol{x}^*$, which is a repelling focus equilibrium.

Figure 1 illustrates three phase resets for the FitzHugh–Nagumo system. Panel (a) shows Γ together with 50 isochrons I_ϑ that are uniformly distributed in phase; the isochrons are shaded in increasingly darker colours for increasing $\vartheta \in [0, 1)$. All isochrons are transverse to Γ and accumulate on $\boldsymbol{x}^*$ sufficiently slowly in a clockwise

https://doi.org/10.1017/S1446181125000082 Published online by Cambridge University Press

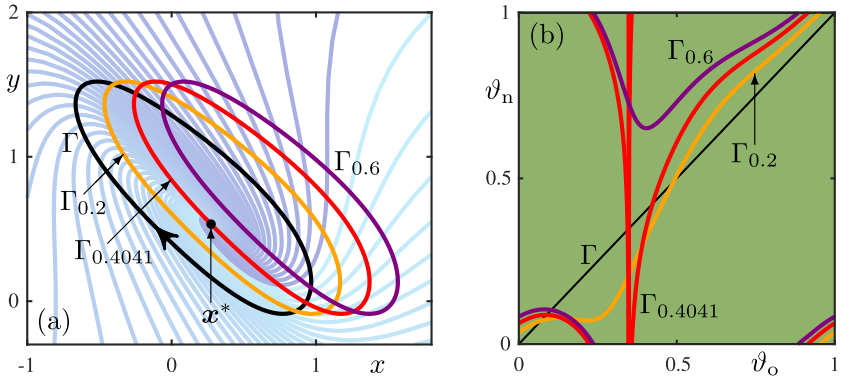

FIGURE 1. Phase resets for the FitzHugh–Nagumo system (2.1) in the x-direction for perturbation amplitudes $A = 0.2$, $A = A_c \approx 0.4041$ and $A = 0.6$. Panel (a) shows the periodic orbit Γ (black) overlayed on 50 isochrons uniformly distributed in phase, coloured from phase 0 (cyan) to 1 (dark blue); also shown are the shifted perturbation sets $\Gamma_{0.2}$ (orange), $\Gamma_{0.4041}$ (red), $\Gamma_{0.6}$ (purple). Panel (b) shows, in matching colours, the resulting three PTCs in the fundamental square where $(\vartheta_o, \vartheta_n) \in [0, 1) \times [0, 1)$ (green shading).

spiralling fashion. A perturbation is applied to each point along Γ, in the horizontal direction (parallel to the x-axis). Hence, Γ is effectively shifted horizontally by the perturbation amplitude A, chosen as $A = 0.2$, $A = A_c \approx 0.4041$ and $A = 0.6$, which gives the shifted perturbation sets labelled $\Gamma_{0.2}$ (orange curve), $\Gamma_{0.4041}$ (red curve) and $\Gamma_{0.6}$ (purple curve), respectively. The resulting three PTCs are shown (with matching colours) in panel (b) for $(\vartheta_o, \vartheta_n) \in [0, 1) \times [0, 1)$, which is the "fundamental square" (green shading) in the $(\vartheta_o, \vartheta_n)$-plane representing the torus $\mathbb{S}^1 \times \mathbb{S}^1$ (by identifying the left and right, and top and bottom sides). The local maxima and minima of the PTCs arise when the perturbation set is tangent to one of the isochrons in the family; in Figure 1(a), such tangencies occur, for example, near the minimum of the shifted perturbation sets (leading to a local maximum of the PTCs).

Note that the perturbation set $\Gamma_{0.4041}$ (red curve) in Figure 1(a) passes exactly through the repelling focus $\boldsymbol{x}^*$ around which the isochrons spiral; indeed, $A = A_c$ is the unique perturbation amplitude with this property, and we refer to it as the critical amplitude A_c. Its relevance is the following. For the perturbation amplitude $A = 0.2$ well before A_c, the perturbation set Γ_A crosses all isochrons, meaning that the PTC covers the full range of $\vartheta_n \in [0, 1)$. Figure 1(b) shows that the PTC for $A = 0.2$ (orange curve) can be viewed as a smooth deformation of the diagonal, which corresponds to a phase reset with $A = 0$, that is, to Γ itself. Note that the PTC for $A = 0.2$ is a continuous smooth curve on the torus $\mathbb{S}^1 \times \mathbb{S}^1$, represented by the fundamental square $[0, 1] \times [0, 1]$. Similarly, when $A = 0.6$ past A_c, the perturbation set Γ_A crosses only a subset of the isochron family. The resulting PTC (purple curve) in Figure 1(b) is again a smooth curve on the torus, but it is now topologically different. Indeed, for $0 \le A < A_c$, the PTC is a $1:1$ torus knot, while for $A > A_c$, it is a $1:0$ torus knot [13, 17]; Winfree called such resets *Type-1* and *Type-0* resets, respectively [22].

https://doi.org/10.1017/S1446181125000082 Published online by Cambridge University Press

Precisely at $A = A_c$, the PTC is singular: the point on Γ with phase $\vartheta_o \approx 0.3484$ resets to $\boldsymbol{x}^*$. In Figure 1(b), the new phase ϑ_n approaches negative infinity in the covering space $\mathbb{R}$ of ϑ_n as this value of ϑ_o is approached from either side. Winfree referred to such an event as *oscillator death* [21] and he realized that it separates the above topologically different cases of PTCs; see also [1, 6]. Remarkably, Winfree was able to construct an idealized sketch of a surface in $(\vartheta_o, A, \vartheta_n)$-space [19, Figure 5], based on approximately 300 experimental data points resulting from phase reset experiments (on yeast cells) at varying phases ϑ_o and perturbation amplitudes A. He observed that his sketch resembles a "spiral staircase rising counterclockwise" and explained that the rotation axis points to an isolated singular stimulus in the (ϑ_o, A)-plane; the singular stimulus is precisely the perturbation with amplitude $A = A_c$ that leads to an interaction with $\boldsymbol{x}^*$. More precisely, Winfree's surface is a helix with its axis the vertical line through the point (ϑ_o, A) with $A = A_c$ and ϑ_o the phase of the point on Γ that resets to $\boldsymbol{x}^*$ for this critical perturbation amplitude. Mathematically speaking, Winfree's spiralling staircase is a ruled surface, which requires that all isochrons are straight rays and hence, *do not spiral* around the phaseless point. However, this is not the typical situation for resets interacting with a single phaseless point, because it requires that the period of the periodic orbit is exactly the time it takes to complete a (small) rotation around the singularity. We suspect that the expansion rate near the phaseless point (relative to the difference in rotation speed) was so strong in Winfree's experiment that the spiralling behaviour was very minimal and could not be resolved in his experiment.

In this paper, we present the FitzHugh–Nagumo system as the typical case of phase resetting in a planar system with a phaseless point. Specifically, the requirement is that the isochrons spiral around this point because there is (generically) a difference between the period of Γ and the rotational speed around the phaseless point. We explained this in a previous work [14], where we studied a family of planar model vector fields, also due to Winfree, for which the isochrons are known explicitly. However, that example has rotational symmetry and, hence, is highly nongeneric. More generally, studies to date of changes in the PTC for varying perturbation amplitudes focused on similar simplified examples [3, 4, 12, 14, 20] that exhibit symmetries to aid in the analysis, or on very realistic models [1, 6, 13, 16–18] with a complexity that obscures the essential underlying mechanisms. In contrast, the FitzHugh–Nagumo system has no symmetries and the difference in rotation speeds around Γ and $\boldsymbol{x}^*$ is sufficiently large to observe the details of the generic changes of the PTC, as the perturbation amplitude A is increased through A_c. This is in contrast to the example of the Van der Pol system that was also studied in [14], but for which the difference in rotation speed turned out to be too small—much like what we suspect was the case in Winfree's experiment [19]. Moreover, the Van der Pol system still has a symmetry; namely, it is invariant under rotation by π around the origin, which is the phaseless point.

In this paper, we show that as A increases through A_c, there is an infinite sequence of *twin tangencies*, where the phase reset is such that the shifted periodic orbit Γ has two separate points of tangency with one and the same isochron. Each such twin tangency

https://doi.org/10.1017/S1446181125000082 Published online by Cambridge University Press

changes how many times the unit interval of ϑ_n is covered by the PTC, which increases to infinity as $A \nearrow A_c$ and then decreases again past $A = A_c$. We are able to identify and illustrate clearly such twin tangencies of the FitzHugh–Nagumo system, which is a representative for a generic planar vector field. Moreover, we discuss how these changes of the PTC (for a given direction of perturbation) are encoded by the geometry of the phase-resetting surface in $(\vartheta_o, A, \vartheta_n)$-space. Colloquially speaking, owing to the spiralling nature of the isochrons near ϑ_n, this surface rolls up around a singular vertical line at $A = A_c$ and the corresponding value of ϑ_o, and this has the observed consequences for the transition of the PTC. We also present a discussion of phase resets with perturbations in different directions (given by an angle φ_d), which are associated with different values of A_c and ϑ_o. To this end, we present the phase-resetting surface in $(\vartheta_o, \varphi_d, \vartheta_n)$-space and show how it changes with the perturbation amplitude A. To obtain these results, we compute isochrons and PTCs with a boundary-value problem setup that was implemented within the package COCO [2] (see [9, 13, 16] for more details).

This paper is organized as follows. In Section 2, we introduce the FitzHugh–Nagumo system and state the specific parameter values we use. Section 3 then introduces its PTC for a perturbation in the positive x-direction and how the PTC is defined as the graph of a function that depends on the perturbation amplitude A. This includes a discussion of the loss of invertibility of this function in Section 3.1 and its changes due to twin tangencies in Section 3.2; the associated phase-resetting surface in $(\vartheta_o, A, \vartheta_n)$-space is introduced and presented in Section 3.3. In Section 4, we discuss the influence of the direction of the perturbation, as represented by the angle φ_d; the five qualitatively different cases of the phase-resetting surface for fixed A are presented and discussed in Section 4.1. We present in Section 5 a discussion and brief outlook on possible future work, and include a short presentation of the computational setup in Appendix A.

2. The FitzHugh–Nagumo system

Winfree [22] studied the FitzHugh–Nagumo system [5, 15] as a typical planar example that cannot be analysed explicitly. He wrote the system as

$$\begin{cases} \dot{x} = c\left(y + x - \frac{1}{3}x^3 + z\right), \\ \dot{y} = -\frac{1}{c}(x - a + b\,y), \end{cases} \tag{2.1}$$

and his interest was in the regime for which this system has an attracting periodic orbit Γ with a repelling focus equilibrium $\boldsymbol{x}^*$ as the single phaseless point. His numerical explorations suggested that the isochron structure is extremely complicated, which was later confirmed with more advanced computational methods [11]. An immediate consequence of such a complex isochron structure is that the FitzHugh–Nagumo system may feature complicated PTCs for phase resets well before the interaction

https://doi.org/10.1017/S1446181125000082 Published online by Cambridge University Press

TABLE 1. The values of the parameters of the FitzHugh–Nagumo system (2.1) that are used throughout.

Winfree's values	No time-scale separation	Off-set from origin
$a = 0.7$ $b = 0.8$	$c = 1$	$z = -0.8$

with the phaseless point [13]. One particular reason for this complexity is a significant difference in time scales between the evolutions of the x- and y-coordinates, as given by the choice for the parameter c [12].

We consider system (2.1) in the same parameter regime as Winfree, but set $c = 1$, so that there is effectively no time-scale separation; moreover, we introduce the off-set $z = -0.8$ to move the equilibrium away from the origin. This choice of parameter values is given in Table 1 and it results in the overall structure of isochrons of the FitzHugh–Nagumo system as illustrated in Figure 1(a). More specifically, the attracting periodic orbit Γ of system (2.1) has $T_\Gamma \approx 10.8329$ and it surrounds the repelling focus $\boldsymbol{x}^* \approx (0.2729, 0.5339)$ with eigenvalues $0.0628 \pm 0.5056\,i$, which constitutes the only point in the phaseless set. As is the convention in the field, we define the zero-phase point $\gamma_0 \approx (0.9660, 0.1345) \in \Gamma$ as the point with the maximum value of the x-coordinate. Since the motion along Γ is clockwise and the rotation period around $\boldsymbol{x}^*$ is larger than T_Γ, the isochrons of Γ spiral around $\boldsymbol{x}^*$ in the clockwise direction [see Figure 1(a)].

3. PTCs for varying perturbation amplitude

The three PTCs illustrated in Figure 1 for the FitzHugh–Nagumo system (2.1) with parameters as in Table 1 are only part of the story of the transition from a 1 : 1 to a 1 : 0 torus knot. As the perturbation amplitude A increases towards A_c, the PTC changes dramatically. To aid the discussion, we define the *phase-resetting function*

$$\mathcal{P}_A : \vartheta_{\mathrm{o}} \in [0, 1) \to \vartheta_{\mathrm{n}} \in [0, 1) \tag{3.1}$$

as the function from the old to the new phase, which has the PTC with given perturbation amplitude $A \geq 0$ as its graph, denoted as graph($\mathcal{P}_A$). Throughout this section, we consider exclusively perturbations in the fixed direction of increasing x, in the form of an instantaneous reset that translates the x-coordinate to the value at distance A in the positive direction, as was done in Figure 1. The phase-resetting function $\mathcal{P}_0$ (in the absence of a perturbation) is the identity, meaning that the PTC for $A = 0$ is the diagonal, labelled Γ in Figure 1(b) and similar figures. In particular, this means that $\mathcal{P}_A$ is invertible when A is sufficiently small. However, when A becomes too large, invertibility of $\mathcal{P}_A$ is lost.

3.1. Loss of invertibility Figure 2 illustrates the loss of invertibility in the style of Figure 1 with the perturbation sets and PTCs for $A = 0.09$ (orange curves), $A = 0.1793$

https://doi.org/10.1017/S1446181125000082 Published online by Cambridge University Press

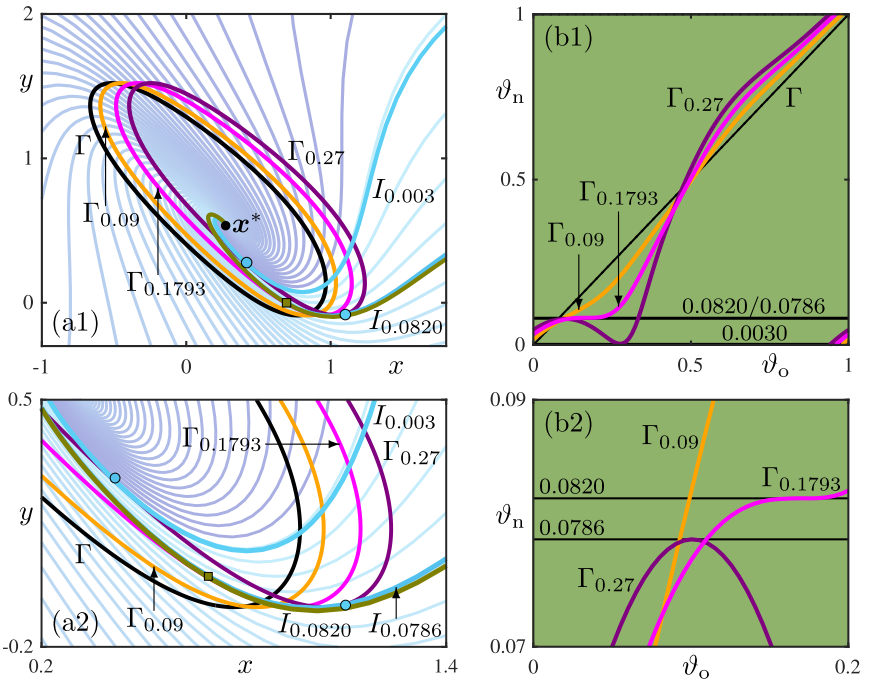

FIGURE 2. Transition through the cubic tangency at $A \approx 0.1793$. Panel (a1) shows Γ (black), $\Gamma_{0.09}$ (orange), $\Gamma_{0.1793}$ (magenta) and $\Gamma_{0.27}$ (purple), with the isochrons $I_{0.0820}$ (olive), $I_{0.0786}$ and $I_{0.0030}$ (both light blue); panel (b1) shows the corresponding three PTCs in matching colours in the fundamental square, where the ϑ_n-values of tangencies are shown as horizontal lines. Panels (a2) and (b2) are respective enlargements near the cubic tangency.

(magenta curves) and $A = 0.27$ (purple curves). Panels (a1) and (a2) of Figure 2 show Γ with the three shifted perturbation sets together with three highlighted isochrons, and panels (b1) and (b2) show the corresponding PTCs. The perturbation set Γ_A for $A = 0.09$ (orange curve) intersects all isochrons transversely and, consequently, $\mathcal{P}_A$ is invertible and the PTC is monotonically increasing. At $A \approx 0.1793$, the perturbation set (magenta curve) has a cubic tangency with the isochron $I_{0.0820}$, which means that the PTC has an inflection point at the value $\vartheta_n = 0.0820$; see the enlargement panels (a2) and (b2). For larger values of A, the perturbation set Γ_A has quadratic tangencies with two different isochrons; for the case $A = 0.27$ (purple curves) shown in Figure 2, these are $I_{0.0786}$ and $I_{0.0030}$. As a consequence, the PTC is no longer invertible: for $A = 0.27$, it has a local maximum at $\vartheta_n = 0.0786$ and a local minimum at $\vartheta_n = 0.0030$. Indeed, Figure 2 clearly illustrates that the loss of invertibility of the PTC is due to the cubic tangency of the perturbation set with an isochron; see also [13, 17].

3.2. First and last twin tangency As A is increased further towards A_c, the local maximum of the PTC moves up in ϑ_n and its local minimum moves down. Since

https://doi.org/10.1017/S1446181125000082 Published online by Cambridge University Press

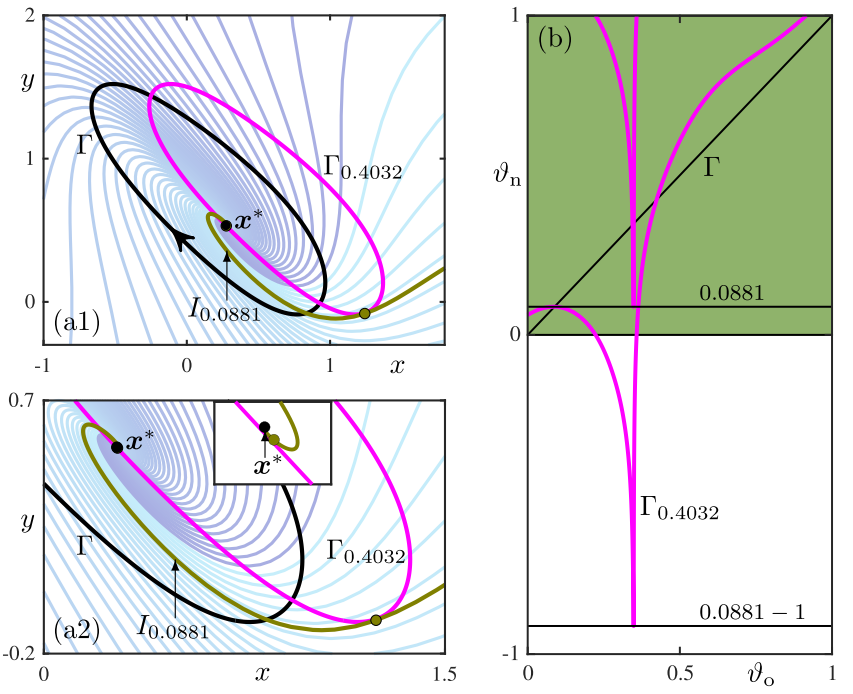

FIGURE 3. The first twin tangency at $A \approx 0.4032 < A_c$. Panel (a1) shows Γ (black) with $\Gamma_{0.4032}$ (magenta) and the isochron $I_{0.0881}$ (olive); and panel (a2) with its inset show successive enlargements near the twin tangency points. The corresponding PTC is shown in panel (b) in the fundamental square (green shading) and as a single smooth curve over the extended ϑ_n-range of $[-1, 1]$.

ϑ_n is taken modulo 1 on the fundamental square, the local maximum and minimum eventually have equal values, which marks a transition in terms of how many times the full range of $\vartheta_n \in [0, 1)$ is covered by $\mathcal{P}_A$ and, hence, the PTC. Geometrically, when viewed in the phase plane, this means that the perturbation set has (quadratic) tangencies with two isochrons that lie increasingly further apart in the family, until their phase difference reaches 0.5; these two isochrons at which the tangencies occur then come closer together and eventually become one and the same isochron. We call this a *twin tangency* and Figure 3 illustrates the first one as A is increased, which occurs at $A \approx 0.4032$. Panel (a1) shows that $\Gamma_{0.4032}$ (magenta) is tangent to the single isochron $I_{0.0881}$ (olive) at two different points; note from the enlargements in panel (a2) that one of these tangencies is very close to the phaseless point $\boldsymbol{x}^*$. The representation in Figure 3(b) of the PTC over the extended ϑ_n-range $[-1, 1]$ illustrates that its maximum and minimum have a difference of 1 in the covering space and, hence, have the same ϑ_n-value in the fundamental square. Notice that $\Gamma_{0.4032}$ intersects every isochron precisely three times; equivalently, the PTC in Figure 3(b) covers the ϑ_n-range $[0, 1)$ of the torus precisely three times. The PTC remains a 1 : 1 torus knot, because the overall increase of ϑ_n with $\vartheta_o \in [0, 1)$ is still 1.

https://doi.org/10.1017/S1446181125000082 Published online by Cambridge University Press

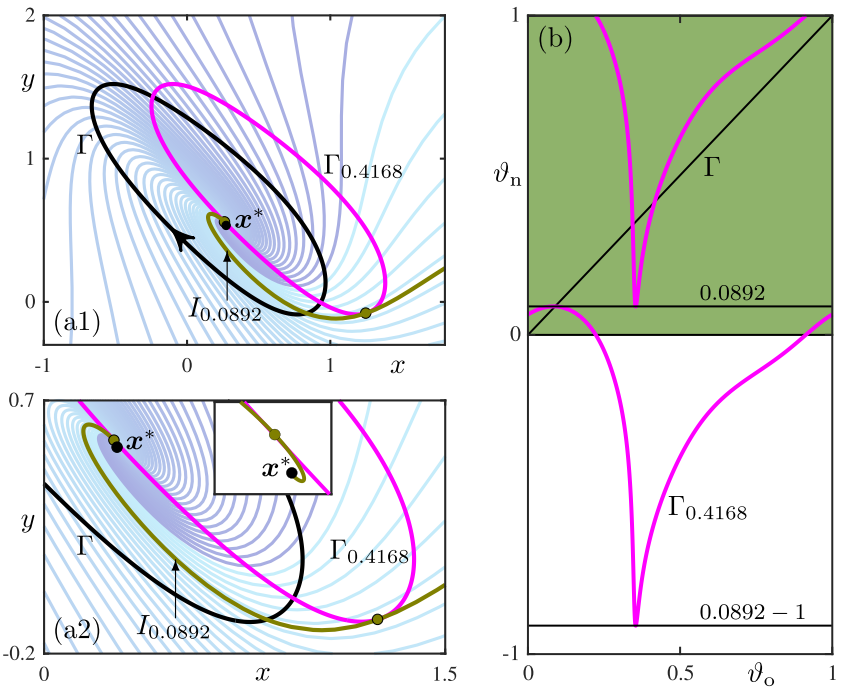

FIGURE 4. The last twin tangency at $A \approx 0.4168 > A_c$. Panel (a1) shows Γ (black) with $\Gamma_{0.4168}$ (cyan) and the isochron $I_{0.0892}$ (olive); and panel (a2) and its inset are successive enlargements near the twin tangency points. The corresponding PTC is shown in panel (b) in the fundamental square (green shading) and as a single smooth curve over the extended ϑ_n-range of $[-1, 1]$.

As Winfree already pointed out [19, 22], the PTC changes topological type from a 1:1 torus knot (Type-1 reset) to a 1:0 torus knot (Type-0 reset) when A is increased through $A = A_c$. For the general case where the isochrons spiral around the phaseless point, as is the case here, the PTC covers the unit ϑ_n-interval of the fundamental square ever more as A is increased further towards A_c [14]. Specifically for system (2.1), the minimum of the PTC moves towards increasingly lower values of ϑ_n, such that there is an infinite sequence of twin tangencies, each increasing the number of coverings of the unit interval by 2. For $A = A_c$, the unit ϑ_n-interval is covered infinitely many times, and for A past the critical value A_c, there is a sequence of twin tangencies in reverse that reduces the number of times the ϑ_n-range $[0, 1)$ is covered. The difference is that, at each twin tangency for $A > A_c$, the perturbation set Γ_A now crosses all isochrons exactly an even number of times. Figure 4 illustrates the last twin tangency of this reverse sequence in the style of Figure 3. As panels (a1) and (a2) of Figure 4 show, the perturbation set $\Gamma_{0.4168}$ (magenta) has two points of quadratic tangency with one and the same isochron $I_{0.0892}$ (olive). Note that, compared with the first twin tangency, the perturbation set and the second tangency point is now "on the other side" of the

https://doi.org/10.1017/S1446181125000082 Published online by Cambridge University Press

phaseless point $\boldsymbol{x}^*$. The PTC in Figure 4(b) is now a 1:0 torus knot that covers $[0, 1)$ exactly twice. After this last twin tangency, for $A > 0.4168$, the PTC loses surjectivity and no longer covers the full range of ϑ_n: the transition through A_c is complete (see the case for $A = 0.6$ in Figure 1(b)).

3.3. Phase-resetting surface near its singularity The entire transition of the PTC through A_c can be represented geometrically by the *phase-resetting surface* consisting of the PTCs for any A. More formally, we now consider the function $\mathcal{P}(\vartheta_\mathrm{o}, A) := \mathcal{P}_A(\vartheta_\mathrm{o})$ over the $(\vartheta_\mathrm{o}, A)$-plane, and the phase-resetting surface of system (2.1) in $(\vartheta_\mathrm{o}, A, \vartheta_\mathrm{n})$-space is $\mathrm{graph}(\mathcal{P}) = \{\mathrm{graph}(\mathcal{P}_A) \mid A \in \mathbb{R}^{\geq 0}\}$. This surface is shown in Figure 5(a). Specifically, we plot the phase-resetting surface over the extended ϑ_n-range $[-1, 2]$, so that, effectively, three copies or sheets are shown. Our focus here is on a neighbourhood of the singular parameter point S given by $A = A_c \approx 0.4041$ and $\vartheta_\mathrm{o} \approx 0.3484$, for which the corresponding point on the periodic orbit Γ maps exactly to $\boldsymbol{x}^*$. In $(\vartheta_\mathrm{o}, A, \vartheta_\mathrm{n})$-space, this parameter point S gives rise to a singular vertical line, and the phase-resetting surface spirals around it. To aid in its interpretation, Figure 5(a) also shows two lifts each of three PTCs: the PTC for $\Gamma_{0.35}$ (orange), which is a 1:1 torus knot; the singular PTC for $\Gamma_{0.4041}$ (red) with singularity at S; and the PTC for $\Gamma_{0.45}$ (purple), which is a 1:0 torus knot.

Figure 5(b) shows a very different surface: the one that is swept out by the isochrons when they are shown in (x, y, ϑ)-space in terms of their ϑ-value; here, we also show three copies over the extended ϑ-range $[-1, 2]$. This isochron surface was generated and rendered from the 50 computed isochrons, which are highlighted on the surface for $\vartheta \in [0, 1)$. The focus is on a region near the phaseless point $\boldsymbol{x}^*$, which similarly gives rise to a singular vertical line around which the isochrons spiral. Observe the striking similarity between the phase-resetting surface near S in Figure 5(a) and the isochron surface near $\boldsymbol{x}^*$ in panel (b). This is explained by the fact that points $(\vartheta_\mathrm{o}, A)$ near S are mapped smoothly and uniquely to points in the (x, y)-plane near $\boldsymbol{x}^*$ by the "action" of the perturbation map, given by $(\vartheta_\mathrm{o}, A) \mapsto \gamma(\vartheta_\mathrm{o}) + (A, 0)$ with $\gamma(\vartheta_\mathrm{o}) \in \Gamma$. Locally near the singular point S and the phaseless set $\boldsymbol{x}^*$, this perturbation map from the $(\vartheta_\mathrm{o}, A)$-plane to the (x, y)-plane is a bijection [14]. Hence, the phase-resetting surface in Figure 5(a) is the diffeomorphic image of the isochron surface in Figure 5(b) under the local inverse of the perturbation map. In particular, it follows that the level set of the phase-resetting surface for any fixed value of ϑ_n is a spiral that accumulates on (but never reaches) the respective point on the vertical line S. In fact, the surface in Figure 5(a) was rendered from a selection of such spirals, each of which was computed as a curve for a fixed value of ϑ_n.

The spiralling nature of the phase-resetting surface around the line S in $(\vartheta_\mathrm{o}, A, \vartheta_\mathrm{n})$-space is the "geometric encoding" of the fact that the transition of the PTC, as A is increased through A_c, necessarily involves infinite sequences of twin tangencies, as was discussed in Section 3.2. In turn, this is a direct consequence of the spiralling of the isochrons around $\boldsymbol{x}^*$ in the (x, y)-plane. The illustration of this insight in Figure 5 for the FitzHugh–Nagumo system represents the generic case of a planar

https://doi.org/10.1017/S1446181125000082 Published online by Cambridge University Press

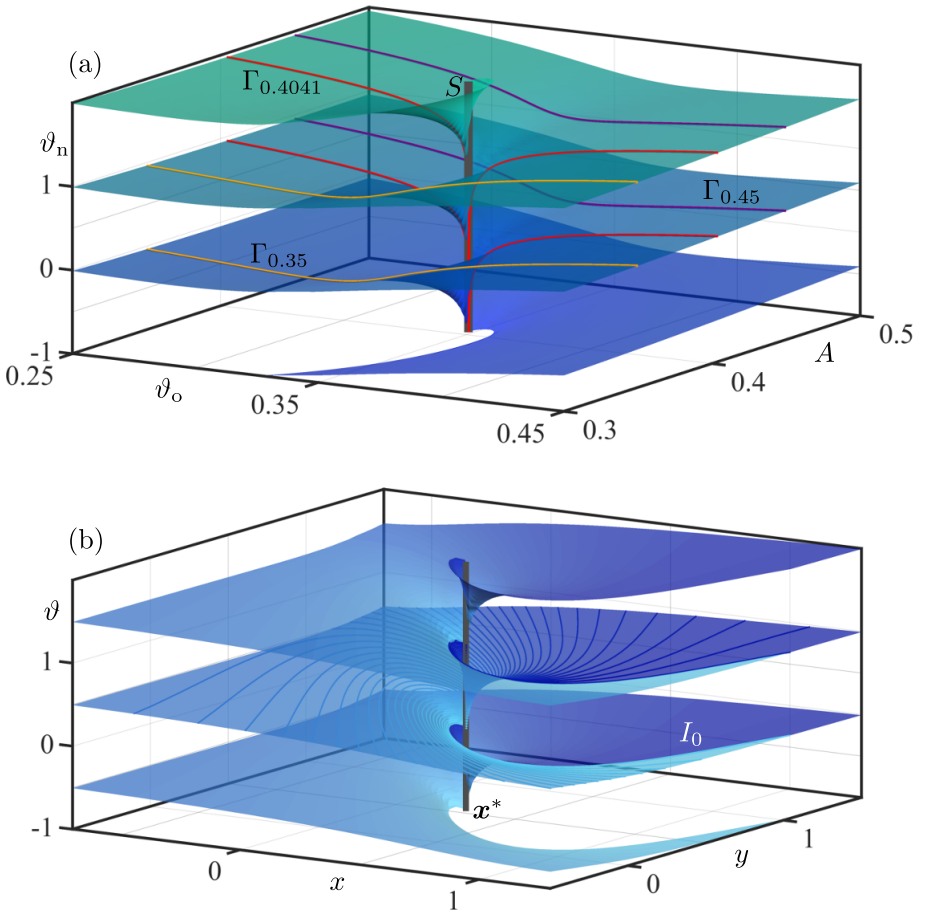

FIGURE 5. Geometry of the phase-resetting surface of system (2.1). Panel (a) shows graph($\mathcal{P}$) in $(\vartheta_o, A, \vartheta_n)$-space near its singular vertical line S over the extended ϑ_n-range $[-1, 2]$; also shown are two lifts each of the PTCs for $\Gamma_{0.35}$ (orange), $\Gamma_{0.4041}$ (red) and $\Gamma_{0.45}$ (purple). Panel (b) shows, for comparison, the surface swept out by the isochrons in (x, y, ϑ)-space near the phaseless set $\boldsymbol{x}^*$, over the extended ϑ-range $[-1, 2]$; the 50 computed isochrons from Figure 1(a) are highlighted for $\vartheta \in [0, 1]$.

vector field; a similar illustration is shown in [14, Figure 8] for a constructed example due to Winfree with rotational symmetry and analytically known isochrons.

4. Varying the direction of perturbation

The application context of the FitzHugh–Nagumo system led us to consider only perturbations in the direction of positive x. However, there is actually no mathematical reason for taking the "traditional" point of view that the direction of the perturbation is fixed. In fact, varying the direction of the perturbation is feasible in experiments,

https://doi.org/10.1017/S1446181125000082 Published online by Cambridge University Press

such as those with self-pulsing semiconductor lasers, where a short external input can be applied to the electrical pump current and/or directly to the optical intensity; and coupled oscillators of any sort, where a perturbation may enter at different strengths for different oscillators. This realization motivates us to extend the earlier definition (3.1) of the phase resetting function $\mathcal{P}_A$ to include the direction of the perturbation as an additional variable [14]. More precisely, we define the unit direction vector

$$\boldsymbol{d} := \boldsymbol{d}(\varphi_{\mathrm{d}}) = \begin{bmatrix} \cos(2\pi\varphi_{\mathrm{d}}) \\ \sin(2\pi\varphi_{\mathrm{d}}) \end{bmatrix}$$

for any direction angle $\varphi_{\mathrm{d}} \in [0, 1)$. (Here and throughout, we consider Euclidean distance.) The definition of $\mathcal{P}_A$ can then be extended to the domain

$$\mathcal{P}_A : [0, 1) \times [0, 1) \to [0, 1); \quad (\vartheta_{\mathrm{o}}, \varphi_{\mathrm{d}}) \mapsto \vartheta_{\mathrm{n}},$$

where the image ϑ_{n} is given by the phase of the isochron that contains the point $\gamma(\vartheta_{\mathrm{o}}) + A\,\boldsymbol{d}(\varphi_{\mathrm{d}})$, resulting from a reset at the point $\gamma(\vartheta_{\mathrm{o}}) \in \Gamma$.

For $\varphi_{\mathrm{d}} = 0$, the unit vector $\boldsymbol{d}(\varphi_{\mathrm{d}})$ is exclusively in the direction of positive x only, which is the case we considered in Section 3. The entire transition scenario of the PTC from 1:1 to 1:0 torus knot we presented is generated solely by the fact that the perturbation set of the periodic orbit moves through the phaseless point $\boldsymbol{x}^*$ as the perturbation amplitude is increased through the critical amplitude A_c. For $\varphi_{\mathrm{d}} = 0$, this happens at $A = A_c \approx 0.4041$ and at the unique point $\gamma(\vartheta_{\mathrm{o}}) \in \Gamma$ of phase $\vartheta_{\mathrm{o}} \approx 0.3484$. However, since Γ surrounds $\boldsymbol{x}^*$, this will also happen for an increasing perturbation amplitude in any direction, albeit for a different value of the critical amplitude A_c and at a different phase ϑ_{o}.

Figure 6 illustrates how the critical perturbation amplitude A_c depends on the perturbation direction $\boldsymbol{d}(\varphi_{\mathrm{d}})$, with $\varphi_{\mathrm{d}} \in [0, 1)$, and the phase $\vartheta_{\mathrm{o}} \in [0, 1)$ at which the reset is applied. Panel (a) shows Γ together with 50 isochrons evenly distributed in phase. We labelled four points on Γ, which are local extrema of the pointwise distance between Γ and $\boldsymbol{x}^*$. Observe that for any $\vartheta_{\mathrm{o}} \in [0, 1)$, the point $\gamma(\vartheta_{\mathrm{o}}) \in \Gamma$ is shifted exactly to $\boldsymbol{x}^*$ by the vector $\boldsymbol{x}^* - \gamma(\vartheta_{\mathrm{o}})$; in other words, $\gamma(\vartheta_{\mathrm{o}})$ resets to $\boldsymbol{x}^*$ for the perturbation with amplitude $A_c = \|\boldsymbol{x}^* - \gamma(\vartheta_{\mathrm{o}})\|$ in the unique direction $\boldsymbol{d} = (\boldsymbol{x}^* - \gamma(\vartheta_{\mathrm{o}}))/\|\boldsymbol{x}^* - \gamma(\vartheta_{\mathrm{o}})\|$. In particular, the critical perturbation amplitude A_c achieves a local maximum or minimum when viewed as a function of ϑ_{o} or, alternatively, as a function of the angle φ_{d} of $\boldsymbol{d}$ as defined above. These two graphs are also shown in Figure 6: A_c as a function of $\vartheta_{\mathrm{o}} \in [0, 1)$ in panel (b) and A_c as a function of $\varphi_{\mathrm{d}} \in [0, 1)$ in panel (c). The extrema of each graph have the same A_c-values and we first discuss how they divide the A_c-axis into five different ranges. Section 4.1 then presents and discusses the corresponding five phase-resetting surfaces, which are shown in Figures 7–11.

The critical perturbation amplitude has a global minimum of $A_c \approx 0.2805$, at $\vartheta_{\mathrm{o}} \approx 0.2981$ and at $\varphi_{\mathrm{d}} \approx 0.1324$, given by the points labelled f_1 in panels (a), (b) and (c) of Figure 6. Hence, any phase reset, in any direction, with perturbation amplitude

https://doi.org/10.1017/S1446181125000082 Published online by Cambridge University Press

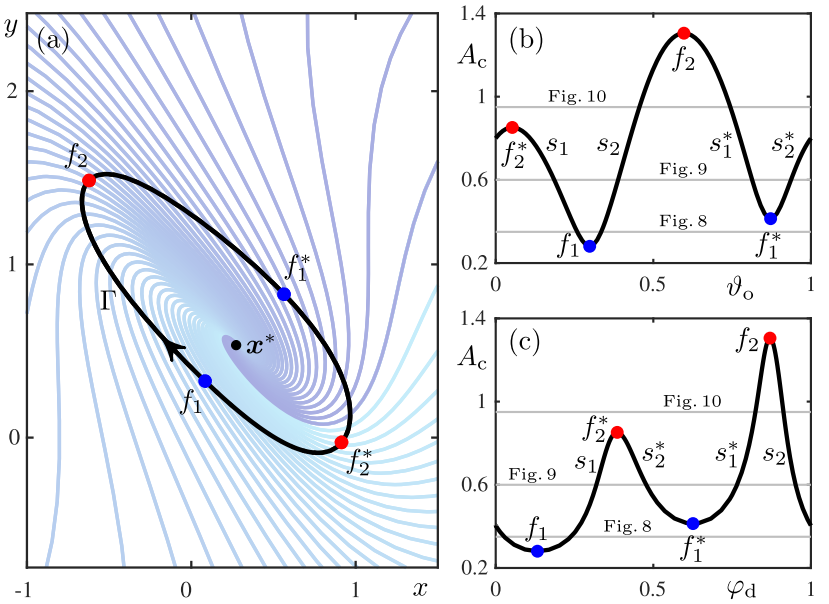

FIGURE 6. Determining the critical perturbation amplitude A_c. Panel (a) shows Γ (black curve) with 50 isochrons evenly distributed in phase and the points labelled f_1, f_1^* (blue) and f_2, f_2^* (red) marked on Γ that lie respectively at (locally) minimal and maximal distances from the source $\boldsymbol{x}^*$. Panels (b) and (c) show the graphs of A_c as a function of ϑ_o and φ_d, respectively, with the branches labelled s_1, s_1^*, s_2 and s_2^* giving the values of ϑ_o and φ_d that achieve singular phase resets for a chosen A_c; the three horizontal lines at $A = 0.35$, $A = 0.6$ and $A = 0.95$ thus identify the singular points shown in Figures 8, 9 and 10, respectively.

$0 \le A < 0.2805$, leads to a PTC that is a 1 : 1 torus knot, because the effect is a small shift of Γ that involves no interaction with $\boldsymbol{x}^*$. Similarly, A_c has a global maximum of $A_c \approx 1.3051$, labelled f_2 in Figure 6, at $\vartheta_o \approx 0.5971$ and at $\varphi_d \approx 0.8702$. Any phase reset, in any direction, with perturbation amplitude $A > 1.3051$ leads to a PTC that is a 1 : 0 torus knot, because the perturbed orbit no longer encloses $\boldsymbol{x}^*$. However, for any perturbation amplitude A in the range $[0.2805, 1.3051]$, there exists a direction angle $\varphi_d \in [0, 1)$ such that PTC has a discontinuity; this direction angle is generically not unique.

The existing pairs (ϑ_o, φ_d) that lead to a singular phase reset are given by the intersection points of the graphs in Figures 6(b) and 6(c) with a horizontal line at the selected value of A_c; each such intersection point lies on one of four branches labelled s_1, s_2, s_1^* and s_2^*. How many there are depends on the level of A_c relative to the two other extremal points f_1^* and f_2^*: a local minimum and a local maximum of the distance from $\boldsymbol{x}^*$ of $A_c \approx 0.4134$ and $A_c \approx 0.8519$, respectively. For any phase reset with perturbation amplitude A in the range $(0.2805, 0.4134)$, the horizontal line with $A_c = A$ intersects only the branches s_1 and s_2; for $A \in (0.4134, 0.8519)$, it intersects all four branches; and for $A \in (0.8519, 1.3051)$, it intersects only the branches s_2 and s_1^*.

https://doi.org/10.1017/S1446181125000082 Published online by Cambridge University Press

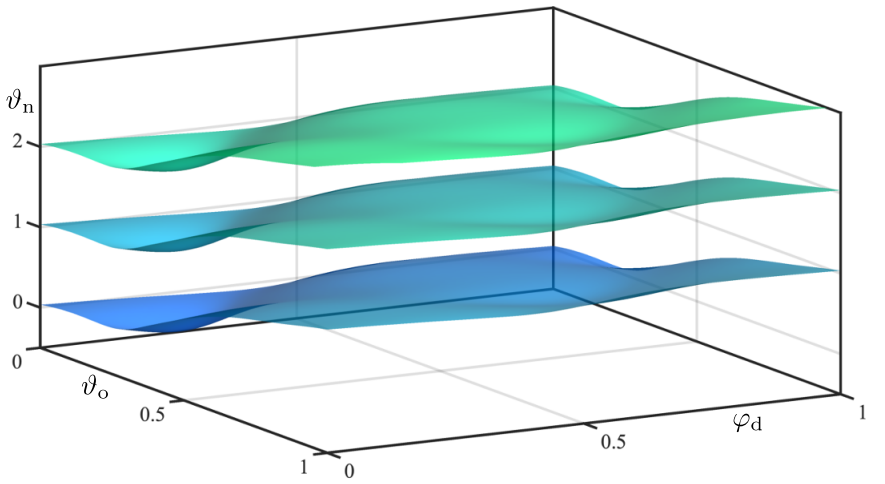

FIGURE 7. Three copies of the phase-resetting surface graph($\mathcal{P}_A$) of system (2.1) shown in $(\vartheta_o, \varphi_d, \vartheta_n)$-space for $\vartheta_n \in [-0.5, 2.5]$ with $A = 0.2$.

Hence, in these ranges, there are two, four and again two particular phases along Γ that reset to $\boldsymbol{x}^*$, provided the associated specific direction angle $\varphi_d \in [0, 1)$ is selected. Each such reset to $\boldsymbol{x}^*$ corresponds to a singularity where the phase reset is not defined; the three horizontal lines indicate the representative values of A we chose in Figures 8–10 to present the corresponding phase-resetting surfaces with singularities.

4.1. Phase-resetting surface for fixed A To illustrate the influence of the direction $\boldsymbol{d}$ of the perturbation, we now consider graph($\mathcal{P}_A$) in $(\vartheta_o, \varphi_d, \vartheta_n)$-space for different values of the perturbation amplitude A. As we discussed above, there are five different generic cases, corresponding to the five A-ranges generated by the values of A_c at the four extrema f_1, f_1^*, f_2 and f_2^*. They are presented in Figures 7–11, where we show three copies or sheets of graph($\mathcal{P}_A$) over the extended ϑ_n-range $[-0.5, 2.5]$.

Figure 7 shows the phase-resetting surface graph($\mathcal{P}_A$) for $A = 0.2$, representing the A-interval $[0, 0.2805)$. Here, the PTC for any φ_d is a 1 : 1 torus knot, which means that the three sheets of graph($\mathcal{P}_A$) are tilted so that the value of ϑ_n increases by 1 as ϑ_o varies from 0 to 1.

Figure 8 shows the situation for $A = 0.35$, representing $A \in (0.2805, 0.4134)$. Panel (a) shows three sheets of graph($\mathcal{P}_A$) in $(\vartheta_o, \varphi_d, \vartheta_n)$-space with the PTCs for the φ_d-values 0.2 and 0.5, panel (b) provides a "top-down" view in projection onto the (ϑ_o, φ_d)-plane, and the two PTCs are shown in panel (c) on the fundamental square. As Figure 8(a) shows, the three sheets of graph($\mathcal{P}_A$) now all wrap around two singular vertical lines labelled s_1 and s_2; these singularities are at $(\vartheta_o, \varphi_d) \approx (0.2585, 0.2372)$ and $(\vartheta_o, \varphi_d) \approx (0.3346, 0.0258)$, and they are created, for increasing A, when the global minimum f_1 at $A_c \approx 0.2805$ is passed in Figures 6(b) and 6(c), so that the branches s_1 and s_2 are intersected. As Figure 8(b) illustrates with a top view, there

https://doi.org/10.1017/S1446181125000082 Published online by Cambridge University Press

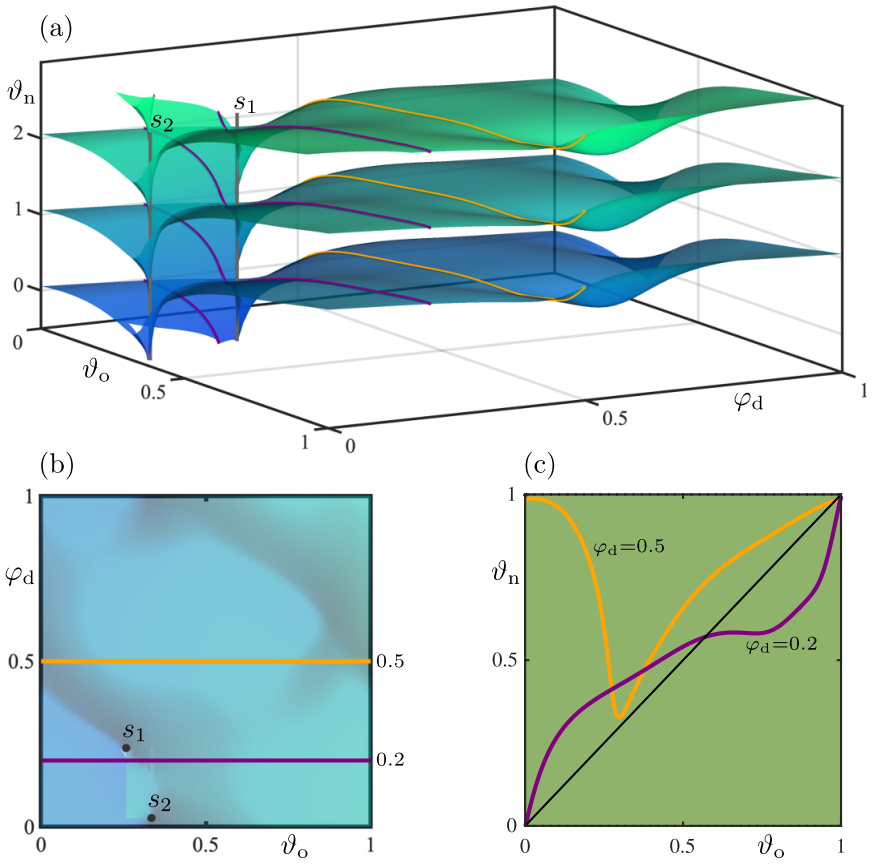

FIGURE 8. Panel (a) shows three copies of the phase-resetting surface graph($\mathcal{P}_A$) of system (2.1) in $(\vartheta_o, \varphi_d, \vartheta_n)$-space for $\vartheta_n \in [-0.5, 2.5]$ with $A = 0.35$, featuring two singularities s_1 and s_2 (grey vertical lines); also shown are the two PTCs for $\varphi_d = 0.2$ (purple) and $\varphi_d = 0.5$ (orange). Panel (b) is a projection of panel (a) onto the (ϑ_o, φ_d)-plane and panel (c) shows the two PTCs on the fundamental square (green shading) of the $(\vartheta_o, \vartheta_n)$-plane.

is now the "window" $(0.0258, 0.2372)$ of φ_d-values in between their "singular" values corresponding to s_1 and s_2, for which the PTC is already a $1:0$ torus knot; for the complement $\varphi_d \in [0, 1) \setminus [0.0258, 0.2372]$, the PTC is still a $1:1$ torus knot. The PTCs for $\varphi_d = 0.2$ and $\varphi_d = 0.5$ in panel (c) are representative examples of these two cases. Exactly for the φ_d-values of the singularities s_1 and s_2, the PTC has a discontinuity as the one for $A = A_c$ shown in Figure 1(b).

Figure 9 shows the phase-resetting surface graph($\mathcal{P}_A$) for $A = 0.6$, which is representative for the A-interval $(0.4134, 0.8519)$, where one finds the four singularities s_1, s_2, s_1^* and s_2^*. Consequently, PTCs without discontinuities for this A-range are found in four φ_d-ranges. The singularities s_1 and s_2 are now at $(\vartheta_o, \varphi_d) \approx (0.1857, 0.3188)$

https://doi.org/10.1017/S1446181125000082 Published online by Cambridge University Press

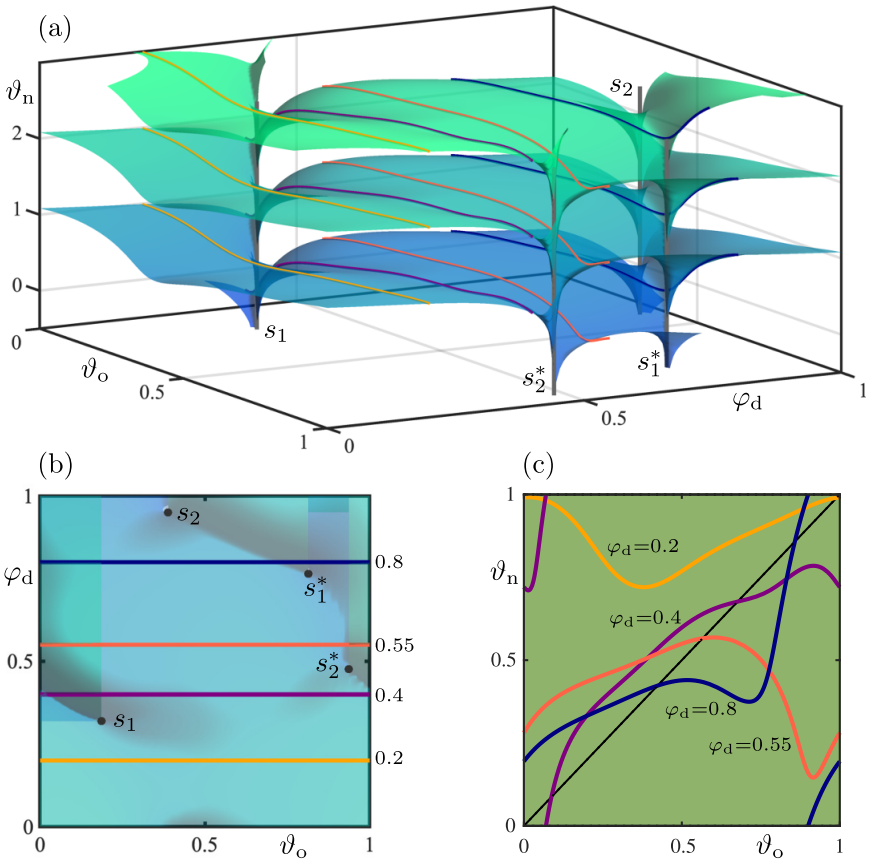

FIGURE 9. Panel (a) shows three copies of the phase-resetting surface graph($\mathcal{P}_A$) of system (2.1) in $(\vartheta_o, \varphi_d, \vartheta_n)$-space for $\vartheta_n \in [-0.5, 2.5]$ with $A = 0.6$, featuring four singularities s_1, s_2, s_1^* and s_2^* (grey vertical lines); also shown are the four PTCs for $\varphi_d = 0.2$ (orange), $\varphi_d = 0.4$ (purple), $\varphi_d = 0.55$ (red) and $\varphi_d = 0.8$ (blue). Panel (b) is a projection of panel (a) onto the (ϑ_o, φ_d)-plane and panel (c) shows the four PTCs on the fundamental square (green shading) of the $(\vartheta_o, \vartheta_n)$-plane.

and $(\vartheta_o, \varphi_d) \approx (0.3883, 0.9508)$, respectively. Moreover, there are two additional singularities s_1^* and s_2^* at $(\vartheta_o, \varphi_d) \approx (0.7651, 0.8135)$ and $(\vartheta_o, \varphi_d) \approx (0.9368, 0.4768)$, respectively. The phase-resetting surface graph($\mathcal{P}_A$) in Figure 9(a) now wraps around all four singular vertical lines s_1, s_2, s_1^* and s_2^*. Resets in directions corresponding to the associated singular φ_d-values lead to discontinuous PTCs. As the top view in panel (b) shows, there are now two "windows" of φ_d-values for which the PTC is already a 1:0 torus knot: the one between s_1 and s_2 for $\varphi_d \in (0.9508 - 1, 0.3188)$, which is wider than in Figure 7, and there is also a second window between s_1^* and s_2^* for $\varphi_d \in (0.4768, 0.8135)$. The PTCs for $\varphi_d = 0.2$ and $\varphi_d = 0.55$ in Figure 9(c) are representative examples for these two φ_d-ranges of 1:0 torus knots. In the two

https://doi.org/10.1017/S1446181125000082 Published online by Cambridge University Press

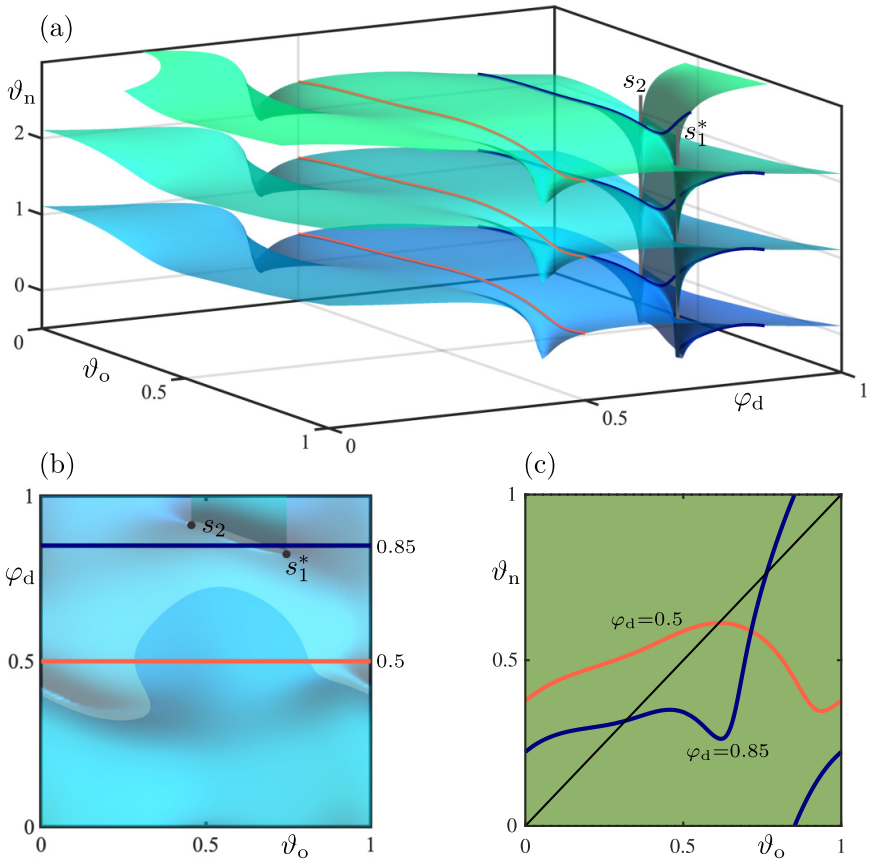

FIGURE 10. Panel (a) shows three copies of the phase-resetting surface graph($\mathcal{P}_A$) of system (2.1) in $(\vartheta_o, \varphi_d, \vartheta_n)$-space for $\vartheta_n \in [-0.5, 2.5]$ with $A = 0.95$, featuring two singularities s_1^* and s_2 (grey vertical lines); also shown are the two PTCs for $\varphi_d = 0.5$ (red) and $\varphi_d = 0.85$ (blue). Panel (b) is a projection of panel (a) onto the (ϑ_o, φ_d)-plane and panel (c) shows the two PTCs on the fundamental square (green shading) of the $(\vartheta_o, \vartheta_n)$-plane.

complementary φ_d-ranges, however, the PTC is still a 1:1 torus knot, such as the PTCs for $\varphi_d = 0.4$ and $\varphi_d = 0.8$ in panel (c).

As A is increased, the singular points s_1 and s_2^* move closer together, and they merge and disappear at the local maximum f_2^* at $A_c \approx 0.8519$. Figure 10(a) shows the phase-resetting surface graph($\mathcal{P}_A$) for $A = 0.95$, which is representative for the A-interval $(0.8519, 1.3051)$. Again, only two singularities remain, namely, s_1^* and s_2 at $(0.7445, 0.8236)$ and $(0.4559, 0.9126)$, respectively. The geometry of the phase-resetting surface graph($\mathcal{P}_A$) in panel (a) looks again like that in Figure 8(a), but the difference is that the PTC is now a 1:0 torus knot for almost all values of φ_d, except for the φ_d-range $(0.8236, 0.9126)$ in between s_1^* and s_2; see Figures 10(b) and 10(c) for the two PTCs for the φ_d-values 0.5 and 0.85 that are representatives of these two cases.

https://doi.org/10.1017/S1446181125000082 Published online by Cambridge University Press

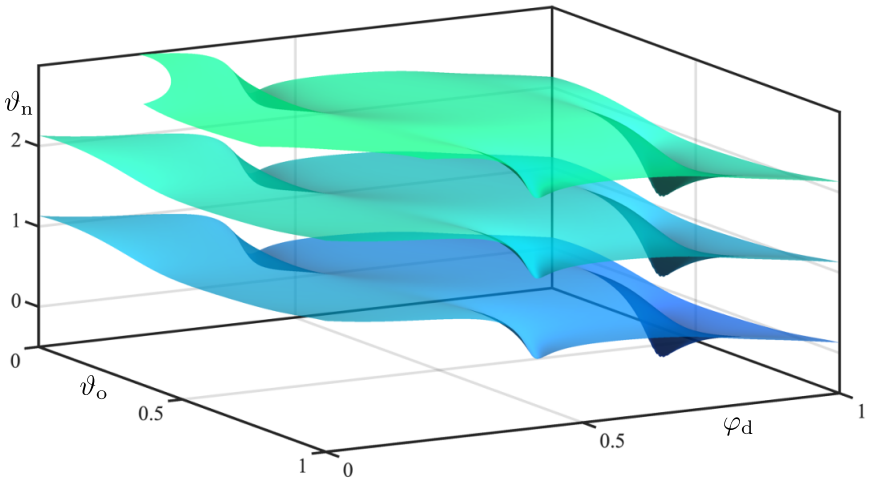

FIGURE 11. Three copies of the phase-resetting surface graph($\mathcal{P}_A$) of system (2.1) shown in $(\vartheta_o, \varphi_d, \vartheta_n)$-space for $\vartheta_n \in [-0.5, 2.5]$ with $A = 0.95$.

As A is increased further through the global maximum f_2 at $A_c \approx 1.3051$, also s_1^* and s_2 disappear and graph($\mathcal{P}_A$) is as shown in Figure 11 for the representative value $A = 1.4$. Here, the three sheets shown are such that there is no increase of ϑ_n when ϑ_o varies from 0 to 1 and, hence, all PTCs are 1 : 0 torus knots. Notice, however, that the three sheets are just tilted differently compared with the three sheets in Figure 7, for which all PTCs are 1 : 1 torus knots. In Figure 11, the value of ϑ_n increases by one as the direction angle φ_d, rather than the old phase ϑ_o, varies from 0 to 1.

5. Conclusion and outlook

We studied phase resetting in the FitzHugh–Nagumo system (2.1), with a stable periodic orbit Γ surrounding a repelling focus $\boldsymbol{x}^*$, which is the only point not in the basin of attraction. Perturbations at phase ϑ_o, with amplitude A and in the direction $\boldsymbol{d}(\varphi_d)$, result in a new phase ϑ_n. We considered first the perturbations in the direction of increasing x, which is "standard" for the FitzHugh–Nagumo system. The phase transition curve is the graph of the function $\mathcal{P}_A(\vartheta_o)$ that "records" the phase ϑ_n after a perturbation at the point $\gamma(\vartheta_o) \in \Gamma$ of strength A. The information of all PTCs can be represented by the phase-resetting surface, which is the graph of the function $\mathcal{P}(\vartheta_o, A) = \mathcal{P}_A(\vartheta_o)$, where A is also viewed as an input. This surface in $(\vartheta_o, A, \vartheta_n)$-space effectively provides an atlas of phase resetting: each PTC is a "slice" through graph($\mathcal{P}$) for the corresponding amplitude A. The phase-resetting surface has a singularity S when the perturbation moves a point on Γ exactly to the phaseless set $\boldsymbol{x}^*$. As Winfree already pointed out, moving the PTC across such a singularity changes it from being a 1 : 1 to a 1 : 0 torus knot, or vice versa, while at the critical amplitude A_c,

https://doi.org/10.1017/S1446181125000082 Published online by Cambridge University Press

the PTC is discontinuous. Owing to the spiralling nature of the isochrons near $\boldsymbol{x}^*$, the phase-resetting surface graph($\mathcal{P}$) wraps around a vertical line at the singular point S. This explains the existence of twin tangencies during the transition through such a "spiralling" singularity, whereby the number of coverings of the fundamental ϑ_n-interval $[0, 1)$ by the PTC first increases and then decreases; we identified and illustrated such twin tangencies of the FitzHugh–Nagumo system.

We also considered the influence of the direction angle φ_d on the PTC. To this end, we computed the phase-resetting surface graph($\mathcal{P}_A$) of the FitzHugh–Nagumo system (2.1) as a function of both ϑ_o and φ_d, which we showed for five representative values of the perturbation amplitude A. The transition with increasing A of the phase-resetting surface graph($\mathcal{P}_A$) in $(\vartheta_o, \varphi_d, \vartheta_n)$-space, which we illustrated in Figures 7–11, is typical for the situation where a convex periodic orbit Γ of a planar vector field surrounds a single phaseless point $\boldsymbol{x}^*$ in the form of a repelling focus equilibrium. The aspects of what we mean by typical are: (1) the speed of rotation around Γ and locally around $\boldsymbol{x}^*$ are different, so that the isochrons spiral into $\boldsymbol{x}^*$; (2) there are two minima and two maxima of the distance $\|\boldsymbol{x}^* - \gamma(\vartheta_o)\|$ of $\boldsymbol{x}^*$ from any point on Γ; and (3) these are in general position (do not have the same values). The FitzHugh–Nagumo system (2.1) is also typical in that its isochrons and PTC are not known analytically and need to be found numerically. By solving suitably formulated multi-segment boundary value problems, we computed a sufficient number of "slices", from which the respective phase-resetting surfaces were then rendered (see the Appendix and [13, 14] for more details on the computational setup).

We remark that the example of the Van der Pol system we discussed in [14] is not typical or generic: due to its invariance under rotation by π, the two minima and the maxima of the distance from the phaseless set are identical. Hence, one does not encounter the intermediate cases with just two singularities that we showed in Figures 8 and 10. Moreover, we found that the rotation of the isochrons near $\boldsymbol{x}^*$, while nonzero, is not pronounced enough in the Van der Pol system to observe properly the wrapping of the phase-resetting surface around vertical lines of singularities. This can be considered a "shortcoming" of the Van der Pol example, which the FitzHugh–Nagumo system does not have. While we focused on how the PTC changes, we mention that one can also consider the directional transition curve (DTC), obtained by considering ϑ_n as a function of φ_d for fixed ϑ_o and A. There is an interesting duality between the PTC and the DTC in terms of its properties near the singularity, which is discussed in considerable detail in [14].

The results we presented here for the FitzHugh–Nagumo system (2.1) are typical, but there are other generic scenarios one may encounter in planar vector fields. First of all, when the phaseless point $\boldsymbol{x}^*$ is very close to a convex periodic orbit Γ surrounding it, the distance $\|\boldsymbol{x}^* - \gamma(\vartheta_o)\|$ may only have a single minimum and a single maximum. Moreover, Γ might not be convex, which could lead to the existence of more than two pairs of (local) minima and maxima of the distance, which are again, generically, in general position. The transition for increasing A of the phase-resetting surface graph($\mathcal{P}_A$) in $(\vartheta_o, \varphi_d, \vartheta_n)$-space through such different sequences of minima

https://doi.org/10.1017/S1446181125000082 Published online by Cambridge University Press

and maxima follows immediately from the arguments we presented here. A more interesting situation is that the phaseless set inside Γ no longer consists of a single point. For example, it could be a disk bounded by a repelling periodic orbit or be the closure of the stable manifold of a saddle equilibrium (see [8, 9] for such examples). In either case, the PTC will be discontinuous at more than just a single point. The associated consequences for the phase-resetting surface can be investigated in the geometric spirit we adopted here, but this remains an interesting subject for future research. Finally, a challenging subject of our ongoing research concerns phase resetting in higher-dimensional systems. The issue here is that the basin boundary of the attracting periodic orbit under consideration may be very complicated; in particular, it will contain the (generally higher-dimensional) stable manifolds of any saddle equilibria and periodic orbits.

Acknowledgements

We thank Peter Langfield for helpful discussions and the anonymous referees for their constructive comments.

Appendix A. Boundary value problem formulation for isochrons and phase resets

Isochrons and phase-resetting curves cannot be derived analytically for a typical system and, hence, need to be computed numerically. We employ a multi-segment boundary value problem (BVP) approach to compute different objects as outlined below. The code for the computation of isochrons of planar systems, implemented in the Matlab-based package COCO [2], is freely available with a detailed tutorial in the Supplementary Material of [9]. Details of the related computation of phase resetting curves can be found in [13].

The key idea of the BVP approach is to implement the relationship between ϑ_{o} and ϑ_{n} given by the phase-resetting function $\mathcal{P}_A$ from (3.1) for given amplitude A and perturbation direction $\boldsymbol{d} = \boldsymbol{d}(\varphi_{\mathrm{d}})$ from (4). Our computational setup is illustrated in Figure 12 for the FitzHugh–Nagumo system (2.1) with $\boldsymbol{d} = \boldsymbol{d}(0) = (1, 0)^T$. Its key ingredient is an orbit segment $\boldsymbol{u} = \{\boldsymbol{u}(s) \mid s \in [0, 1]\}$ that satisfies the differential equation

$$\boldsymbol{u}' = K\, T_\Gamma\, \boldsymbol{F}(\boldsymbol{u}), \tag{A.1}$$

where $\boldsymbol{F} : \mathbb{R}^2 \to \mathbb{R}^2$ is sufficiently smooth and time is rescaled by a multiple $K \in \mathbb{N}$ of the period T_Γ of the attracting periodic orbit Γ under consideration. Note that Γ with its period T_Γ, zero-phase point γ_0 and stable Floquet bundle can be obtained with a standard BVP setup [9, 16]. Hence, we assume here that they are known.

The orbit segment $\boldsymbol{u}$ is subject to the boundary conditions

$$\boldsymbol{u}(0) = \gamma_{\vartheta_{\mathrm{o}}} + A\, \boldsymbol{d}(\varphi_{\mathrm{d}}) = \gamma_{\vartheta_{\mathrm{o}}} + A\, [\cos(\varphi_{\mathrm{d}}), \sin(\varphi_{\mathrm{d}})], \tag{A.2}$$

$$\boldsymbol{u}(1) = \gamma_{\vartheta_{\mathrm{n}}} + \eta\, \mathbf{v}_{\vartheta_{\mathrm{n}}}, \tag{A.3}$$

https://doi.org/10.1017/S1446181125000082 Published online by Cambridge University Press

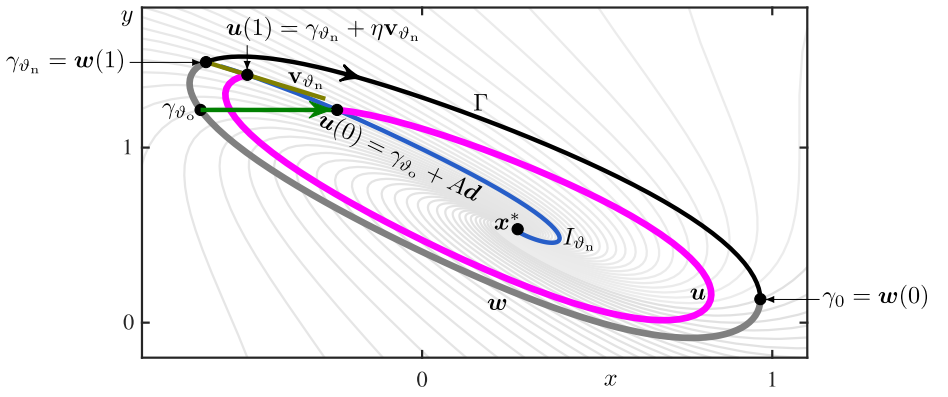

FIGURE 12. The BVP setup with the orbit segments $\boldsymbol{u}$ (magenta) and $\boldsymbol{w}$ (grey) relating ϑ_o and ϑ_n, illustrated for the FitzHugh–Nagumo system (2.1) with $\varphi_\mathrm{d} = 0$, giving $\mathcal{P}_A(0.5) = 0.6$ for $A \approx 0.3899$. Also shown are the periodic orbit Γ (black) with the points γ_0, $\gamma_{\vartheta_\mathrm{o}}$ and $\gamma_{\vartheta_\mathrm{n}}$, the stable unit Floquet vector $\mathbf{v}_{\vartheta_\mathrm{n}}$ (olive), and 50 isochrons (light grey) uniformly distributed in phase, where the respective branch of I_{ϑ_n} (blue) is highlighted.

where $\mathbf{v}_{\vartheta_\mathrm{n}}$ is the stable unit Floquet vector at $\gamma_{\vartheta_\mathrm{n}} \in \Gamma$ and the distance $\eta \in \mathbb{R}$ from $\gamma_{\vartheta_\mathrm{n}}$ is small. While $\gamma_{\vartheta_\mathrm{o}}$ is taken as input here, the point $\gamma_{\vartheta_\mathrm{n}}$ is given by its phase shift ϑ_n from γ_0, as determined by the auxiliary orbit segment $\boldsymbol{w}$ with $\boldsymbol{w}(0) = \gamma_0$ and $\boldsymbol{w}(1) = \gamma_{\vartheta_\mathrm{n}}$; finding $\gamma_{\vartheta_\mathrm{n}}$ in this way also means that $\mathbf{v}_{\vartheta_\mathrm{n}}$ is known; see [13] for further details.

When η in (A.3) is sufficiently small, $\boldsymbol{u}(1)$ lies on the isochron I_{ϑ_n} to good approximation; this can be achieved by choosing K in (A.1) large enough. Since the integration time is a multiple of T_Γ, the point $\boldsymbol{u}(0)$ also lies on I_{ϑ_n} to good approximation. In Figure 12, we show the case $K = 1$ with a rather large η for illustrative purposes; specifically, we have that $\mathcal{P}_A(0.5) = 0.6$ for $A \approx 0.3899$.

The BVP (A.1)–(A.3) for $\boldsymbol{u}$ is very flexible and allows the computation of different kinds of objects of interest. The isochron I_{ϑ_n} (of a planar system) for fixed ϑ_n is traced out by $\boldsymbol{u}(0)$ as an arclength parametrized curve by performing a continuation in η; here, we ensure that η is always sufficiently small by increasing K as necessary [9, 11, 16]. Moreover, when choosing ϑ_o as the continuation parameter for fixed φ_d and A, one generates the PTC as the graph $(\vartheta_\mathrm{o}, \mathcal{P}_A(\vartheta_\mathrm{o}))$. Finally, a phase-resetting surface can be constructed and rendered from a sequence of PTCs computed for a suitable set of values of either A or φ_d; it is also possible to construct it from curves at given "heights", which can be found by fixing ϑ_n at a suitable set of values.

References

[1] E. N. Best, "Null space in the Hodgkin–Huxley equations. A critical test," *Biophys. J.* **27** (1979) 87–104; doi:10.1016/S0006-3495(79)85204-2.

[2] H. Dankowicz and F. Schilder, *Recipes for continuation* (SIAM Publishing, Philadelphia, PA, 2013); doi:10.1137/1.9781611972573.

https://doi.org/10.1017/S1446181125000082 Published online by Cambridge University Press

[3] G. B. Ermentrout, L. Glass and B. E. Oldeman, "The shape of phase-resetting curves in oscillators with a saddle node on an invariant circle bifurcation," *Neural Comput.* **24** (2012) 3111–3125; doi:10.1162/NECO_a_00370.

[4] G. B. Ermentrout and D. H. Terman, *Mathematical foundations of neuroscience*, Volume 35 of Interdiscip. Appl. Math. (Springer, New York, 2010); doi:10.1007/978-0-387-87708-2.

[5] R. FitzHugh, "Impulses and physiological states in theoretical models of nerve membrane," *Biophys. J.* **1** (1961) 445–466; doi:10.1016/S0006-3495(61)86902-6.

[6] L. Glass and A. T. Winfree, "Discontinuities in phase-resetting experiments," *Am. J. Physiol. Regul. Integr. Comp. Physiol.* **246** (1984) R251–R258; doi:10.1152/ajpregu.1984.246.2.R251.

[7] J. Guckenheimer, "Isochrons and phaseless sets," *J. Math. Biol.* **1** (1975) 259–273; doi:10.1007/BF01273747.

[8] J. Hannam, B. Krauskopf and H. M. Osinga, "Global isochrons of a planar system near a phaseless set with saddle equilibria," *Eur. Phys. J. Spec. Top.* **225** (2016) 2645–2654; doi:10.1140/epjst/e2016-60072-4.

[9] J. Hannam, B. Krauskopf and H. M. Osinga, "Isochron foliations and global bifurcations: a case study," *Trans. Math. Appl.* **6** (2022) tnac002; with COCO code and tutorial for computing isochrons of planar systems as supplementary material; doi:10.1093/imatrm/tnac002.

[10] M. W. Hirsch, C. C. Pugh and M. Shub, *Invariant manifolds*, Volume 583 of Lecture Notes in Math. (Springer, Berlin–Heidelberg, 1977); doi:10.1007/BFb0092042.

[11] P. Langfield, B. Krauskopf and H. M. Osinga, "Solving Winfree's puzzle: the isochrons in the FitzHugh–Nagumo model," *Chaos* **24** (2014) Article ID: 013131; doi:10.1063/1.4867877.

[12] P. Langfield, B. Krauskopf and H. M. Osinga, "Forward-time and backward-time isochrons and their interactions," *SIAM J. Appl. Dyn. Syst.* **14** (2015) 1418–1453; doi:10.1137/15M1010191.

[13] P. Langfield, B. Krauskopf and H. M. Osinga, "A continuation approach to computing phase resetting curves," in: *Advances in dynamics, optimization and computation. SON 2020*, Volume 304 of Stud. Syst. Decis. Control (eds. O. Junge, O. Schütze, G. Froyland, S. Ober-Blöbaum and K. Padberg-Gehle) (Springer-Verlag, Cham, Switzerland, 2020) 3–30; doi:10.1007/978-3-030-51264-4_1.

[14] K. H. Lee, N. G. R. Broderick, B. Krauskopf and H. M. Osinga, "Phase response to arbitrary perturbations: geometric insights and resetting surfaces," *Discrete Contin. Dyn. Syst. Ser. B* **30** (2025) 2094–2134; doi:10.3934/dcdsb.2024140.

[15] J. Nagumo, S. Arimoto and S. Yoshizawa, "An active pulse transmission line simulating nerve axon," *Proc. IRE* **50** (1962) 2061–2070; doi:10.1109/JRPROC.1962.288235.

[16] H. M. Osinga and J. Moehlis, "Continuation-based computation of global isochrons," *SIAM J. Appl. Dyn. Syst.* **9** (2010) 1201–1228; doi:10.1137/090777244.

[17] A. Pérez-Cervera, T. M. Seara and G. Huguet, "A geometric approach to phase response curves and its numerical computation through the parameterization method," *J. Nonlinear Sci.* **29** (2019) 2877–2910; doi:10.1007/s00332-019-09561-4.

[18] N. W. Schultheiss, A. A. Prinz and R. J. Butera, *Phase response curves in neuroscience: theory, experiment, and analysis*, Volume 6 of Comput. Neurosci. (Springer, New York, 2012); doi:10.1007/978-1-4614-0739-3.

[19] A. T. Winfree, "Time and timelessness in biological clocks," in: *Temporal aspects of therapeutics*, Volume 2 of ALZA Conf. Ser. (eds. J. Urquhart and F. E. Yates) (Springer, Boston, MA, 1973) 35–49; doi:10.1007/978-1-4684-2847-6_4.

[20] A. T. Winfree, "Patterns of phase compromise in biological cycles," *J. Math. Biol.* **1** (1974) 73–93; doi:10.1007/BF02339491.

[21] A. T. Winfree, "Sudden cardiac death: a problem in topology," *Sci. Amer.* **248** (1983) 144–161; doi:10.1038/scientificamerican0583-144.

[22] A. T. Winfree, *The geometry of biological time*, 2nd edn, Volume 12 of Interdiscip. Appl. Math. (IAM) (Springer, New York, 2001); doi:10.1007/978-1-4757-3484-3.